

AD-A142 220

EFFECT OF REFRACTORY ELEMENTS ON THE COHERENCY STRAIN
AND FLOW STRESS ON NICKEL-BASE SUPERALLOYS(U)
RENSSELAER POLYTECHNIC INST TROY NY M NAIK ET AL.

1/1

UNCLASSIFIED

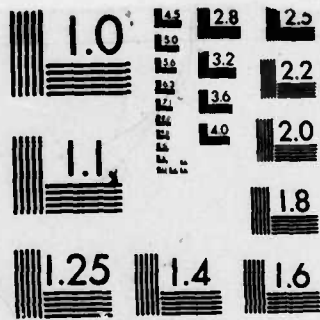
JUN 84 TR-16 N00014-76-C-0458

F/G 11/6

NL



END
DATE
FILMED
7-84
DTIC



MICROCOPY RESOLUTION TEST CHART
NATIONAL BUREAU OF STANDARDS-1963-A

12

AD-A142 220
DTIC FILE COPY

REPORT DOCUMENTATION PAGE		READ INSTRUCTIONS BEFORE COMPLETING FORM
1. REPORT NUMBER TECHNICAL REPORT NO. 16	2. GOVT ACCESSION NO. ----	3. RECIPIENT'S CATALOG NUMBER ----
4. TITLE (and Subtitle) EFFECT OF REFRACTORY ELEMENTS ON THE COHERENCY STRAIN AND FLOW STRESS ON NICKEL-BASE SUPERALLOYS		5. TYPE OF REPORT & PERIOD COVERED Technical Report
7. AUTHOR(s) Makund Naik and George S. Ansell		6. PERFORMING ORG. REPORT NUMBER ----
9. PERFORMING ORGANIZATION NAME AND ADDRESS Rensselaer Polytechnic Institute Troy, New York 12181		8. CONTRACT OR GRANT NUMBER(s) N00014-76-C-0458 NR 031-689/8-6-82 (430)
11. CONTROLLING OFFICE NAME AND ADDRESS ----		10. PROGRAM ELEMENT, PROJECT, TASK AREA & WORK UNIT NUMBERS ----
14. MONITORING AGENCY NAME & ADDRESS (if different from Controlling Office) METALLURGY PROGRAM, OFFICE OF NAVAL RESEARCH Department of the Navy 800 N. Quincy St., Arlington, VA 22217		12. REPORT DATE June 1984
		13. NUMBER OF PAGES 12
		15. SECURITY CLASS. (of this report) Unclassified
16. DISTRIBUTION STATEMENT (of this Report) UNLIMITED		15a. DECLASSIFICATION/DOWNGRADING SCHEDULE ----
<div style="border: 1px solid black; padding: 5px; display: inline-block;"> <p>DISTRIBUTION STATEMENT A Approved for public release Distribution Unlimited</p> </div>		
17. DISTRIBUTION STATEMENT (of the abstract entered in Block 20, if different from Report) ----		
18. SUPPLEMENTARY NOTES -----		
19. KEY WORDS (Continue on reverse side if necessary and identify by block number) Nickel-base alloys, superalloys, coherency strain, misfit, refractory elements, γ - γ' , mismatch, antiphase boundary, flow stress.		
20. ABSTRACT (Continue on reverse side if necessary and identify by block number) (see attached page)		

DTIC
ELECTE
JUN 19 1984
S * D
B

gammaABSTRACT

Various refractory elements from groups IVB, VB and VIB are used in nickel-base superalloys to increase their mechanical strength and service life at high temperatures. Group IVB and VB metals partition primarily to γ' , dilate the γ' structure and increase its antiphase boundary energy. Group VIB metals partition primarily to the γ matrix and dilate the γ lattice and decrease its stacking fault energy. The alteration of the lattice parameters of γ and γ' by these elements changes the effective coherency strain. Molybdenum and tungsten also reduce the solubility of aluminum in the matrix, whereas titanium reduces the solubility of molybdenum in the γ' precipitate. These interactions affect the resulting volume fraction of γ' and the $\gamma - \gamma'$ mismatch. Deformation in high coherency alloys proceeds by dislocation-particle bypass through Orowan bowing, whereas in low coherency alloys, deformation requires dislocation-particle shear (APB shear, S/ISF-S/ESF shear). The flow stress in Ni-15Cr-Ti-Al-Mo alloys is shown to be mainly a function of coherency strain at all temperatures.

Accession For	
NTIS GRA&I	<input checked="" type="checkbox"/>
DTIC TAB	<input type="checkbox"/>
Unannounced	<input type="checkbox"/>
Justification	
By _____	
Distribution/	
Availability Codes	
Dist	Avail and/or Special
A-1	

Technical Report No. 16

to

OFFICE OF NAVAL RESEARCH

Contract No. N00014-76-C-0458

Task Nr. 031-689/8-6-82 (430)

Entitled

EFFECT OF REFRACTORY ELEMENTS ON THE COHERENCY STRAIN
AND FLOW STRESS ON NICKEL-BASE SUPERALLOYS

Submitted by

Makund Naik and George S. Ansell
Rensselaer Polytechnic Institute
Troy, New York 12181

June 1984

Reproduction in whole or in part is permitted for any purpose of the United States Government. Distribution of this document is unlimited.

84 06 18 055



AMERICAN SOCIETY FOR METALS
Metals Park, Ohio 44073

Metals/Materials Technology Series

**EFFECT OF REFRACTORY ELEMENTS
ON THE COHERENCY STRAIN
AND FLOW STRESS ON NICKEL-BASE
SUPERALLOYS**

Makund Naik and George S. Ansell
Rensselaer Polytechnic Institute
Troy, New York

1984 ASM Conference on Refractory Alloying
Elements in Superalloys — Effects and
Availability
Rio de Janeiro, Brazil
6-13 April 1984

8402-013

84 06 18 055

AMERICAN SOCIETY FOR METALS
1190 Park Circle West

Metals Technology Series

No part of this paper may be reproduced, stored in a retrieval system, or transmitted, in any form or by any means, electronic, mechanical, photocopying, recording, or otherwise, without the prior written permission of the publisher.

Nothing contained in this paper is to be construed as a grant of any right of manufacture, sale, or use in connection with any method, process, apparatus, product, or composition, whether or not covered by letters patent or registered trademark, nor as a defense against liability for the infringement of letters patent or registered trademark.

SAN: 204-7586
Copyright 1984 American Society for Metals
All rights reserved

84 08 18 025

8402-013

EFFECT OF REFRACTORY ELEMENTS ON THE COHERENCY STRAIN AND FLOW STRESS ON NICKEL-BASE SUPERALLOYS

Makund Naik and George S. Ansell

Rensselaer Polytechnic Institute
Troy, New York

ABSTRACT

Various refractory elements from groups IVB, VB and VIB are used in nickel-base superalloys to increase their mechanical strength and service life at high temperatures. Group IVB and VB metals partition primarily to γ' , dilate the γ' structure and increase its antiphase boundary energy. Group VIB metals partition primarily to the γ matrix and dilate the γ lattice and decrease its stacking fault energy. The alteration of the lattice parameters of γ and γ' by these elements changes the effective coherency strain. Molybdenum and tungsten also reduce the solubility of aluminum in the matrix, whereas titanium reduces the solubility of molybdenum in the γ' precipitate. These interactions affect the resulting volume fraction of γ' and the $\gamma - \gamma'$ mismatch. Deformation in high coherency alloys proceeds by dislocation-particle bypass through Orowan bowing, whereas in low coherency alloys, deformation requires dislocation-particle shear (APB shear, S/ISF-S/ESF shear). The flow stress in Ni-15Cr-Ti-Al-Mo alloys is shown to be mainly a function of coherency strain at all temperatures.

NICKEL-BASE SUPERALLOYS derive their strength from solid solution strengthening and a variety of two-phase strengthening mechanisms. Coherency strain is one of the two-phase strengthening mechanisms that affects not only the mechanical strength of the alloy but also the morphology and stability of the precipitate at elevated temperature.

Coherency strains (or the $\gamma - \gamma'$ mismatch or $\gamma - \gamma'$ misfit in nickel-base superalloys) are elastic strains in precipitation hardenable alloys which arise to accommodate the difference in atomic volumes of the precipitate and the matrix. A fully coherent precipitate requires that the matrix and the precipitate lattices match exactly and corresponding planes

and directions be continuous across the matrix-precipitate interface. The degree of coherency is represented by the unconstrained mismatch, δ , given by:

$$\delta = \frac{a_0 \gamma' - a_0 \gamma}{a_0 \gamma} \quad (1)$$

Here $a_0 \gamma'$ is the measured lattice parameter of the extracted γ' phase removed from the matrix. The constrained or "in situ" mismatch, ϵ , for the γ' precipitate in γ matrix is related to δ , by,

$$\epsilon = \delta \cdot \frac{1 + \nu}{1 + 2k + \nu(1 - 4k)} \quad (2)$$

where

$$\begin{aligned} \nu &= \text{Poisson's ratio of the precipitate} \\ k &= \frac{\text{shear modulus of the matrix}}{\text{shear modulus of the precipitate.}} \end{aligned}$$

If we assume $\nu = 1/3$, and the moduli of the matrix and precipitate are equal, then $\epsilon = 2/3 \delta$.

There have been a number of theories developed^{1,2,6} to estimate the magnitude of strengthening due to coherency strains. These have assumed the major strengthening factor to be the interaction between glide dislocations and the coherency strain field surrounding the particles. All these theories predict the increment in shear stress ($\Delta\tau$) due to coherency strain obeys a relationship of the type $\Delta\tau \propto \epsilon^{3/2} (r)^{1/2}$, where ϵ is the constrained lattice misfit and r is the mean particle radius. The Gerold-Haberkorn¹ and Gleiter² models differ however in the manner in which the elastic interaction between the strain field of a dislocation and a coherent precipitate is averaged over the array of particles. The major difference between these models, caused by the methods of averaging and the curvature

of the dislocations, is the dependence of $\Delta\tau$ on the volume fraction of precipitate. The equation derived by Gerold and Haberkorn is:

$$\Delta\tau = 3\mu\epsilon \left(\frac{r}{b}\right)^{1/2} \quad (3)$$

and Gleiter's version is:

$$\Delta\tau = 11.8\mu\epsilon \left(\frac{r}{b}\right)^{1/2} f^{5/6} \quad (4)$$

where

- μ = shear modulus of the matrix,
- ϵ = constrained lattice misfit between the particle and the matrix,
- f = volume fraction of precipitate,
- b = Burgers vector, and
- r = mean particle radius.

Brown and Ham's equation is similar to the one derived by Gerold and Haberkorn, only differing by a constant. So these theories predict that the stress to shear a coherent particle increases with the radius in a parabolic manner. In nickel-base alloys the γ' particles have an ordered structure, and to shear them requires more stress. This contribution to the stress is called order strengthening. Coherency and order strengthening are the two major strengthening mechanisms in nickel-base superalloys.

1. EFFECT OF COHERENCY STRAIN

1.a) ON THE GROWTH AND MORPHOLOGY OF γ' - In the initial stages of aging of a Ni-base alloy, the γ' particles are spherical and their growth follows Wagner's law, but on further aging the morphology of γ' changes from spheres to cuboids to cuboidal arrays to finally solid-state dendrites.³ The diameter at which the morphologic transition from spherical to cubical shape occurs is function of the absolute value of $\gamma - \gamma'$ mismatch.^{3,4} The smaller the misfit, the larger is the γ' particle size before which the strain effect dictates the shape. The γ' particles on overaging lose coherency, relaxing the elastic strain mainly by capturing matrix dislocations.⁵ Here, the sign of coherency strain is important. If the $\gamma - \gamma'$ misfit is positive, the compressive hydrostatic stress field around the γ' particle will repel matrix dislocations with edge components. So in alloys with positive misfit, γ' particles can grow into large cuboids without fully losing coherency. In contrast, for alloys with negative misfit, the γ' particles capture matrix dislocations and lose coherency relatively early during growth.

1.b) ON THE DISLOCATION-PARTICLE INTERACTION - Deformation of nickel-base superalloys requires that dislocations either 1) shear the γ' or 2) bypass the γ' particles through Orowan bowing. Generally small γ' particles are sheared, and the stress to shear coherent

particles is given by Eq. (3) or (4). In Fig. 1, curve I schematically describes the stress associated with particle shear for an alloy with a constant volume fraction of precipitate.

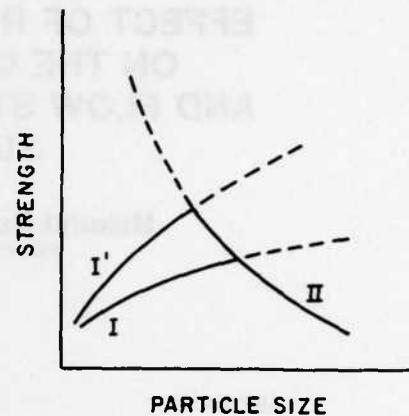


Fig. 1 - Strength vs particle diameter for a particle hardened alloy.

Particle bypass by bowing occurs when the stress required for particle shear reaches or exceeds the Orowan bowing stress (curve II in Fig. 1). Curve I can be raised to I' by strengthening the particles (e.g., by increasing APBE) or by increasing coherency strain. Then dislocation bowing should occur at a smaller particle size. If the particles are non-deformable (e.g., oxide particles in dispersion strengthened alloys), then only particle bypass mechanisms should be observed. If the volume fraction of the particles is raised, both curve I and II will be raised and hence will increase the stress required for both particle shear and bypass mechanisms.

The Orowan loops left behind around the particle after bowing are unstable in the coherency strain field of the particle. On further deformation, the inner loops either shear the particle, or cross-slip and give rise to two prismatic loops. Prismatic cross-slip depends on the amount of misfit and the stacking fault energy of the matrix⁴ and becomes more probable as the stacking fault energy and misfit strain both increase. Prismatic cross-slip has not been observed in nickel-base superalloys containing γ' .

1.c) ON THE STABILITY OF MICROSTRUCTURE - Coherency strains are also important from the standpoint of the stability of γ' particles at elevated temperatures under load as in creep and stress-rupture conditions. Mirkin and Kanchev,⁷ in their investigation of the effect of coherency strain on the stress-rupture life for a series of Ni-Cr-Al alloys found that longer life was correlated with low values of $\gamma - \gamma'$ mismatch. Decreasing the lattice mismatch from 0.2% to zero led to a fifty-fold increase in the stress-rupture life. Maniar et al.⁸ also found that the addition of 5.5% Mo to

a Ni-20Cr-2Ti-1Al alloy decreased the misfit from 0.7% to 0.2% and resulted in an increase in the stress-rupture life. This increase in elevated temperature properties with decreasing misfit was attributed to the effect of misfit strain on the particle stability. If the mismatch is high, so is the corresponding interfacial strain energy. As a result the strengthening phase, hyperfine γ' , will coalesce and grow, weakening the alloy and hence lowering stress-rupture life.¹¹

2. EFFECT OF ALLOYING ADDITIONS IN NICKEL-BASE SUPERALLOYS

The $\gamma - \gamma'$ mismatch, and consequently the coherency strains can be altered by alloying additions such as, titanium, molybdenum and other refractory elements. Besides altering the $\gamma - \gamma'$ mismatch and solid solution strengthening, these metals also affect the chemistry, APBE and amount of γ' , stacking fault energies in γ and γ' , morphology and the amount of various carbides and the formation of TCP phases which, in turn, is reflected in the yield strength and the stress-rupture properties. Here only group IVB, VB, and VIB elements from the Periodic Table (Fig. 2) are

PERIOD ↓	GROUP →		
	IVB	VB	VIB
4	Ti 0.2896	V 0.2697	Cr 0.2573
5	Zr 0.3179	Nb 0.2944	Mo 0.2807
6	Hf 0.3127	Ta 0.2941	W 0.2823

$a_{Ni} = 0.2492 \text{ nm}$
 $a_{Al} = 0.2864 \text{ nm}$

Elements substitute for Al
 Elements substitute for Ni & Al

Fig. 2 - Section of the periodic table showing the substitution behavior and the Goldschmidt radii of the elements. Radii of nickel and aluminum are given for comparison.

discussed because of their commercial importance. First, the effect of these elements on the coherency strain is considered and later, effects on other related structural properties are discussed.

2.a) GROUP IVB AND VB METALS - These two group elements will be discussed together because they all partition mainly to the γ' phase, substituting for Al. The volume fraction of precipitated γ' is proportional to the

amount of hardener content (Ti + Zr + Hf + V + Nb + Ta + Al) in a given nickel base alloy. Nordheim and Grant¹² first observed that the substitution of titanium for aluminum in Ni-20Cr-14.7 at. % Al increased the lattice mismatch. Decker and Mihalisin¹⁴ substituted 2 at. % of various ternary elements for 2 at. % of Al in a Ni-20Cr-14.5 at. % Al alloy and studied their effect on the lattice mismatch and the tensile properties at 760°C. They found that Ta and Nb increased the mismatch but V and Si reduced it. In tensile tests, the alloy with Ta showed maximum yield strength, followed by, V, Nb, and Si. Basically, since the atomic size of the IVB and VB elements is larger (except for vanadium) than that of aluminum, substitution for Al leads to an increase in the mismatch.

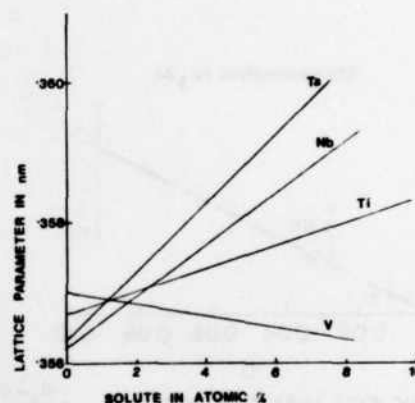


Fig. 3 - Effect of alloying on the lattice parameter of Ni_3Al . (Data taken from Ref. 15(Ta), 37(Nb), 38(Ti) and 39(V)).

Recent results^{15,16} have confirmed that hafnium and tantalum on a per atomic percent basis expand the lattice parameter of γ' most, followed by Nb and Ti (see Fig. 3). No data was found on the effect of Zr and from Guard and Westbrook's³⁹ study, vanadium decreases the γ' lattice parameter. Rawlings and Staton-Bevan¹⁷ from their study of the effect of ternary alloying additions to Ni_3Al , have correlated the increment in the yield strength in polycrystalline Ni_3Al to the atomic size misfit (see Fig. 4a and 4b). Here, atomic size misfit is defined as the fractional difference between the diameters of the alloying atom and the atom for which it substitutes. This effect was observed for stoichiometric as well as Al-rich Ni_3Al . The authors suggested that the substitution for Ni or Al in Ni_3Al was determined by electronic considerations. For the elements that substitute for Al in Ni_3Al , the increment in strength was found to be a function of atomic misfit. If the element substituted for Ni or both Ni and Al in Ni_3Al , then there was no significant strengthening observed, regardless of the atomic misfit.

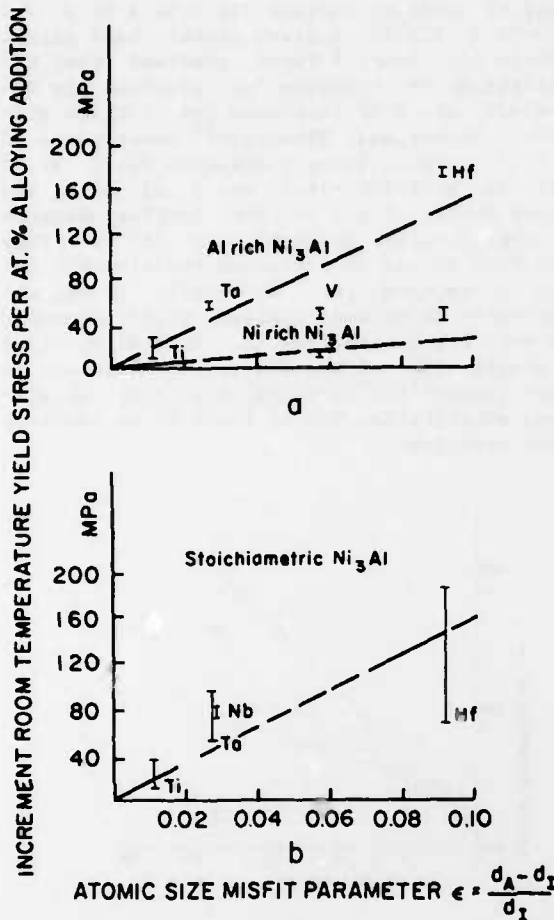


Fig. 4 - The room temperature strengthening of Ni_3Al by elements which substitute for aluminum in a) non-stoichiometric and b) stoichiometric Ni_3Al (Ref. 17).

2.b) GROUP VIB METALS - Group VIB elements (Cr, Mo and W) are also used in Ni-base superalloys. In contrast to group IVB and VB elements, group VIB elements partition to the matrix to varying degrees. So the solid solution strengthening effect of these elements in the Ni-base matrix is more pronounced than that due to group IVB and VB metals. Chromium partitions 10:1 to the matrix relative to the γ' , whereas molybdenum partitions 3:1 to the matrix and tungsten partitions about equally in γ and γ' .²² Of these, chromium is most soluble in the nickel matrix and tungsten the least.³⁰ Fig. 5 shows solid solution strengthening observed in Ni-Cr, Ni-Mo, and Ni-W binary alloys by Pelloux and Grant.²³ Chromium atoms being slightly larger than Ni atoms, its addition dilates the lattice parameter of the matrix. Mo and W also are more potent in expanding the γ matrix because of their larger atomic size. Fig. 6 shows the variation in lattice parameter of binary solid solution Ni-X alloys versus the concentration of X in the alloy.

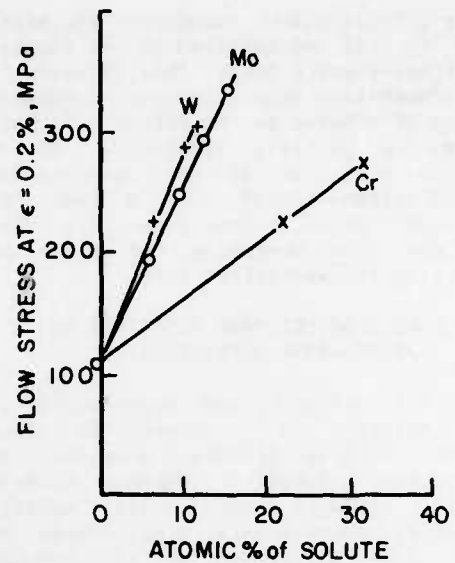


Fig. 5 - The room temperature yield strength vs solid solution content (Ref. 23).

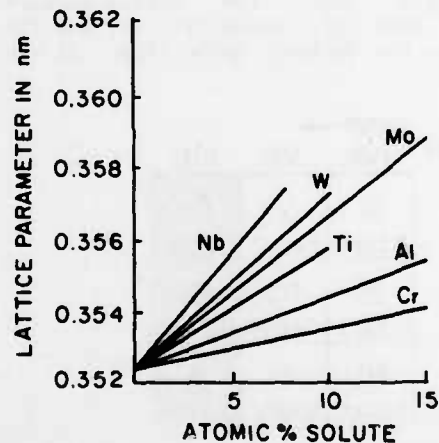


Fig. 6 - The lattice parameter of nickel-base solid solution vs solid solution content (Ref. 41).

There have been a number of studies in which the effect of Mo or W on the microstructure and various mechanical properties of Ni-base alloys was investigated. Havalda^{26,27} from his study of Ni-20Cr-Ti-Al-W alloys concluded that W increases the lattice parameters of both γ and γ' . Because the increment in lattice parameter of the γ is more than that in γ' , W effectively decreases the coherency strain (Fig. 7). The morphology of γ' changed from cuboid to round particles as the lattice mismatch was decreased. Tungsten also retarded the $\gamma' + \eta$ transformation.

Maniar et al⁸⁻¹⁰ have investigated the effect of $\gamma - \gamma'$ mismatch on γ' solvus temperature and stress rupture life. They found that the addition of Mo raises the γ' solvus

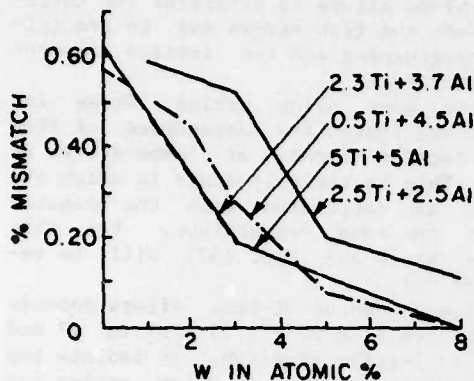


Fig. 7 - Variation in $\gamma - \gamma'$ mismatch with the addition of tungsten to Ni-20Cr-Ti-Al alloys (Ref. 26).

temperature. Molybdenum, by decreasing the lattice misfit was found to increase the creep-rupture life. Loomis et al²⁸ have studied the effect of Mo on γ' precipitation in a Ni-14Cr-Ti-Al alloy series. From this study, it was found that molybdenum reduces the solubility of aluminum in the matrix and hence increases the weight fraction of γ' . Molybdenum also dissolves extensively in γ' in titanium free alloys. Titanium reduces the solubility of Mo in γ' . The effect of molybdenum on the $\gamma - \gamma'$ mismatch is shown in Fig. 8. The $\gamma - \gamma'$ mismatch decreases as more molybdenum is added to the alloy system. Molybdenum, by decreasing the coherency strain, also retards the coarsening of γ' particles on aging.²⁹ When Mo and W, both, are present, their interaction decreases the solubility of aluminum in the nickel-base matrix.³⁰ Molybdenum decreases the solubility of aluminum whereas tungsten increases it. But when Mo and W, both are present, the decrease in the solubility of Al in the matrix is more than the reduction in solubility when only Mo is present.

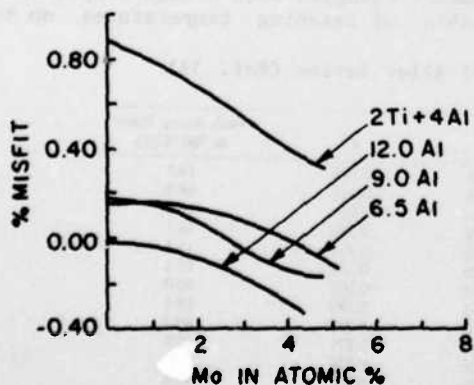


Fig. 8 - Variation in $\gamma - \gamma'$ mismatch with the addition of Mo to Ni-15Cr-Ti-Al alloys (Ref. 28).

2.c) OTHER STRUCTURAL PROPERTIES - Group

IVB and VB elements also strengthen the γ' in another way. By substituting for Al in the ordered structure of γ' , they increase the antiphase boundary energy.^{18,19} The APBE, of the mixed compound $Ni_3(X,Al)$ can be arranged in descending order as:¹⁹ $APBE(Ni_3(Nb,Al)) > APBE(Ni_3(Ti,Al)) > APBE(Ni_3Al)$. The APBE of the following mixed compounds, $APBE(Ni_3(Ta,Al))$ and $APBE(Ni_3(V,Al))$ and $APBE(Ni_3(Hf,Al))$ are probably higher than those containing Nb or Ti. If enough of the Al atoms are replaced with Ti, V, Ta, Hf or Nb atoms, the metastable γ' with $L1_2$ structure may transform into a different phase (DO_{24} for Ti, DO_{22} for V, Ta and Nb). These elements also contribute to the solid-solution strengthening of the γ matrix.

Zirconium and hafnium are believed to have beneficial effect on the mechanical properties of nickel-base superalloys. Zr has a limited solubility in γ' (about 2 at. %) and hafnium is a little more soluble (7 at. %) in γ' .⁴⁰ Because of its large atomic size, Zr is also thought to exist at the grain boundaries and stabilize them.²⁰ Hafnium also substitutes for Mo in MC carbides.²¹ Controlled additions of hafnium in Ni-base alloys change the morphology of eutectic γ' and MC carbides, and as a result improve the ductility and the strength at low and intermediate temperatures.²¹

Chromium serves the purpose that no other refractory metal can serve in Ni-base superalloys. It imparts good oxidation and hot corrosion resistance to these alloys. Indeed, the base composition of most of the commercial superalloys is Ni-10Cr to about Ni-20Cr. All the elements in group IVB, VB and VIB pick up carbon from solution and precipitate as various carbides (MC, $M_{23}C_6$, M_6C , etc., where M denotes above mentioned metals). Usually M in these carbides is Cr, but other reactive metals like Ti and Ta fully or partly substitute for Cr. These elements also have a high electron hole number associated with them, which in greater concentration make Ni-base alloys prone to sigma (or other TCP) phase formation. Another point that merits mentioning here is that, these elements lower the stacking fault energy of the Ni-base matrix. Nickel has the highest stacking fault energy in fcc metals, 235 mJ/m^2 .²⁴ The drop in SFE with Cr content is gradual.²⁵ In the Ni-Mo system, the variation in SFE with Mo is a little more steep.²⁴ In the Ni-W system, there is an initial precipitous drop in SFE, from 235 mJ/m^2 for pure Ni to about 100 mJ/m^2 for Ni -1 at. % W, but then the decrease in SFE with increasing W addition is gradual.²⁴

2.d) DESIGN OF $\gamma - \gamma'$ MISMATCH - The $\gamma - \gamma'$ mismatch in Ni-Al system, where γ is pure nickel (ignoring solid solubility of Al for the sake of computation), and γ' is stoichiometric Ni_3Al is $(a_0\gamma' - a_0Ni)/a_0Ni = 0.0106$. The actual mismatch may be a little less due to the dilation of nickel lattice with larger Al atoms. This mismatch can be varied two ways. First, by the addition of elements

that partition to γ' (e.g., Ti or Nb) and dilate the γ' structure and hence increase the coherency strain. Alternatively, one can add an element that partitions to expand the γ matrix (e.g., Mo or W) and therefore decrease the coherency strain. Elements that partition to γ' and the ones that partition to γ should be balanced to obtain 1) maximum solid solution strengthening in both the phases and 2) adjust the $\gamma - \gamma'$ mismatch close to zero for greater high temperature γ' stability and better creep rupture life albeit with loss of coherency strengthening. To increase the amount of Mo and W in the matrix, the Cr level has to be lowered, which probably lowers its oxidation and hot corrosion resistance. Cobalt addition to nickel increases its lattice parameter and can also be utilized to reduce the $\gamma - \gamma'$ misfit.¹¹

3. COHERENCY STRAIN AND TENSILE STRENGTH

In most investigations of coherency strains, the mismatch is determined at room temperature while the mismatch in service at elevated temperatures may be quite different. Morrow et al³¹ have determined the effect of Mo on the thermal expansion coefficients of Ni-Co-Cr solid solutions and Ni-Cr-Mo-Ti-Al two phase alloys up to 1050°C. They found that molybdenum decreases the coefficient of thermal expansion of both, γ and γ' . Because of the ordered structure of γ' , its thermal expansion coefficient should be smaller than that of the γ matrix and Morrow's data confirms this. The net coefficient of thermal expansion of a two phase alloy is the weighted average of the thermal expansion coefficient of each phase. Titanium, by restricting the solubility of Mo in γ' and, Mo by reducing the solubility of aluminum in the γ matrix, results in an increase in the weight fraction of γ' . An increase in weight fraction of γ' , e.g., by adding aluminum, reduces the thermal expansion coefficient.

Miller and Ansell³² studied the room temperature tensile behavior of a series of

Ni-15Cr-Ti-Al-Mo alloys to determine the correlation between the flow stress due to precipitation strengthening and the lattice mismatch at room temperature.

For the same alloy series Grose and Ansell³³ investigated the dependence of flow stress on lattice mismatch at temperatures up to 800°C. This is the only study in which the flow stress was correlated with the mismatch existing at the same temperature. For this reason this study and Ref. (32) will be reviewed in detail.

The flow stress of Ni-base alloys depends on 1) weight fraction of γ' , 2) APBE in γ' and 3) the $\gamma - \gamma'$ lattice mismatch. To isolate the effect of each variable, an alloy series was designed for which each of these factors could be independently varied keeping the other two variables constant. The base composition was Ni-15%Cr. The hardener content (Ti + Al) was about 7 at. % to get a medium weight fraction of γ' (15-25%) on aging at 760°C. Titanium was used to vary the APBE (it also increased the γ' lattice parameter as a side effect). APBE in Ni-Cr-Ti-Al alloys has been correlated to Ti/Al ratio and the maximum strength due to APBE is obtained when the ratio is about 1.8.¹³ The Ti/Al ratio was varied from zero to 5.4. Molybdenum was used from zero to 5 at. % to expand the lattice parameter of γ and hence to vary the coherency strain. Table I lists the composition of the alloy series. The alloys were separated in four groups based on their coherency strain and APBE properties (see Table 2). Group A and B distinguish high and low APBE alloys possessing high coherency strain. Group C and D, again separate high and low APBE alloys but with low coherency strain. A fifth group of alloys, group E, consists of control alloys to monitor the extent of γ solid solution strengthening. Alloys in this last group are not precipitation hardenable.

Lattice parameter measurements of γ and extracted γ' were obtained using an X-ray diffractometer equipped with a high temperature stage capable of reaching temperatures up to

Table I - Chemical Composition of the Experimental Alloy Series (Ref. 33)

Alloy	Cr	Mo	Al	Ti	B	C	Peak Aging Time at 760 °C(h)
1	14.99	0.00	2.42	4.47	0.026	0.248	16.5
2	15.09	0.99	2.52	4.51	0.026	0.212	69.5
3	15.09	0.00	1.09	5.86	0.026	0.207	16.5
4	15.11	0.15	2.71	4.45	0.026	0.198	16.5
5	15.14	0.52	2.90	4.54	0.026	0.201	16.5
6	14.73	0.12	3.18	5.11	0.026	0.201	63.1
7	15.06	0.37	3.37	5.64	0.026	0.205	60.0
8	15.15	0.00	4.68	2.29	0.031	0.199	69.5
9	15.11	2.96	2.49	4.46	0.032	0.258	69.5
10	15.11	4.98	2.56	4.48	0.027	0.271	195.8
11	15.12	0.00	6.94	0.00	0.026	0.226	69.5
12	15.09	2.97	7.07	0.00	0.026	0.197	41.4
13	14.51	4.99	7.12	0.00	0.032	0.214	69.5
14	14.89	4.88	7.10	0.00	0.024	0.478	69.5
15	14.74	0.00	10.18	0.00	0.021	0.324	—
16	15.09	4.98	0.00	0.00	0.027	0.198	—
17	15.23	0.00	3.19	0.00	0.025	0.047	—
18	15.05	0.00	1.52	2.52	0.026	0.157	—

Table II - Alloy Groups Based on the Coherency Strain and APBE (Ref. 33)

Group Designation	Alloy Numbers	General Properties	γ - γ' Mismatch Range at 25 °C	Ti/Al Ratio (APBE)
Group A	1,2,3 4-7	High Coherency Strain High APBE	$0.77 < \delta < 1.04$ pct	Ti/Al = 1.8
Group B	8	High Coherency Strain Low APBE	$\delta = 0.56$ pct	Ti/Al = 0.5
Group C	9,10	Low Coherency Strain High APBE	$\delta(9) = 0.44$ pct $\delta(10) = 0.16$ pct	Ti/Al = 1.8 $\gamma_{APBE}(10) = 0.2 \text{ Jm}^{-2}$
Group D	11-15	Low Coherency Strain Low APBE	$-0.14 < \delta < 0.06$ pct	Ti/Al = 0 $\gamma_{APBE}(11) = 0.133 \text{ Jm}^{-2}$
Group E	16,17,18	Control—Nonprecipitation hardenable	N.A.	N.A.

1000°C in vacuum. The lattice parameter data for γ and extracted γ' , collected at various temperatures was used to compute the unconstrained lattice mismatch. For a few alloys the constrained mismatch was also obtained directly. Tensile tests were carried out on the solid solution control alloys to determine the matrix flow stress as a function of temperature. For each of the other alloys in the alloy series, room temperature tensile tests in the solutionized condition gave σ_{SS} , the solid solution contribution at room temperature. From σ_{SS} and the variation in flow stress for the appropriate control alloy, the flow stress due to solid solution strengthening, σ_y , for each alloy as a function of temperature was determined. The increment in the yield stress due to the γ' precipitation in peak aged condition, $\Delta\sigma_y$, was then determined by subtracting the solid solution contribution, σ_y , from the observed flow stress of a two phase alloy, σ_y^{max} .

3.a) VARIATION IN COHERENCY STRAIN WITH TEMPERATURE - The expansion behavior of the alloys was separated into two classes. For alloys with type I behavior, $a_0\gamma' > a_0\gamma$ and therefore the mismatch, positive at room temperature, was found to decrease with increasing temperature. (See Fig. 9a and 9b). For the rest of the alloys with type II behavior, $a_0\gamma' < a_0\gamma$, the absolute value of the mismatch increased slowly with increasing temperature (see Fig. 10). From the lattice parameter data at various temperatures, thermal expansion coefficients for γ and γ' in each alloy were computed. The thermal expansion coefficient for γ' was found to be less than that of γ , presumably due to the ordered structure of γ' . The thermal expansion coefficients of γ decreased with increasing Mo addition, confirming Morrow's results (see Fig. 11). The constrained mismatch is related to unconstrained mismatch, by Eq. (2). In this equation, if we assume Poisson's ratio is 1/3 and insensitive to temperature, and that k from Ono and Sterns³⁴ data remains 0.9 over a wide temperature range, the constrained mismatch should be about $2/3 \delta$ throughout. In the case of alloy #6, it was found that at room temperature, $\epsilon = 0.79 \delta$ and at 800°C, $\epsilon = 0.89 \delta$, indicating a small variation in k with

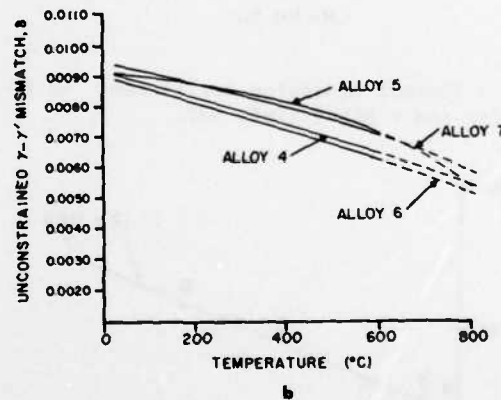
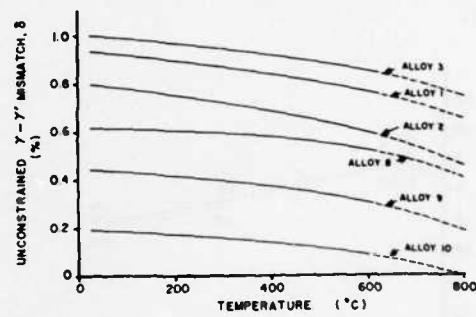


Fig. 9 - The unconstrained $\gamma - \gamma'$ mismatch, δ , as a function of temperature for alloys exhibiting Type I behavior; a) alloys 1-3 and 8-10 and b) alloys 4-7 (Ref. 33).

temperature.

3.b) TENSILE PROPERTIES AT ROOM TEMPERATURE - The flow stress increment, $\Delta\sigma_y$, was found to be proportional to the weight fraction of γ' , for a given mismatch (see Fig. 12). Cornwall et al.³⁵ also reported that the critical resolved shear stress of aged Ni-Al single crystals is approximately linearly proportional to the volume fraction of γ' in the volume fraction range of 0.09 to 0.55. The increase in Ti/Al ratio, and hence increase in δ and APBE for alloys 11, 8, 1 and 3 where the weight fraction of γ' was essentially constant, results in a substantial increase in the flow

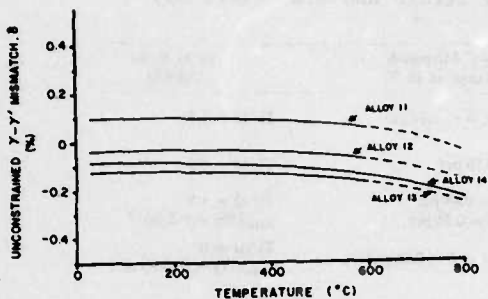


Fig. 10 - The unconstrained $\gamma - \gamma'$ mismatch as a function of temperature for Type II alloys (Ref. 33).

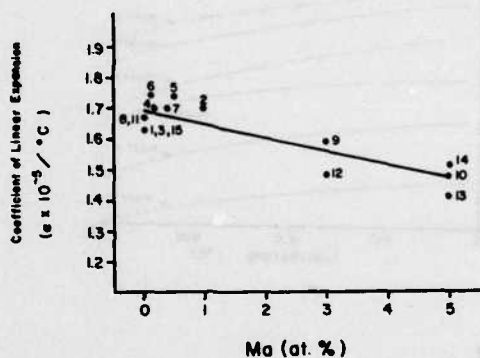


Fig. 11 - Thermal expansion coefficient vs Mo content for the γ phase (Ref. 33).

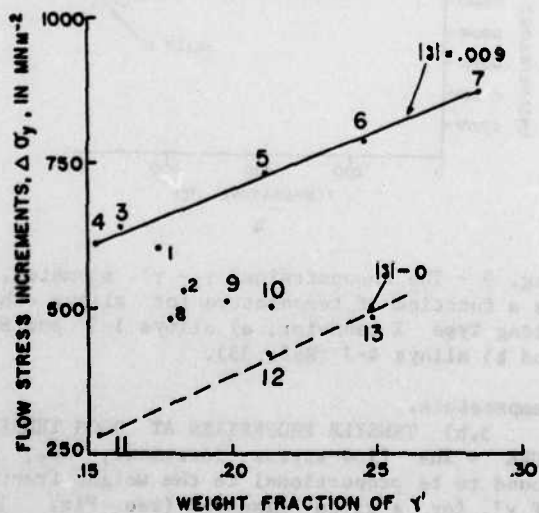


Fig. 12 - Flow stress increment, $\Delta\sigma_y$, vs weight fraction of γ' at room temperature (Ref. 32).

stress increment. In this group of alloys, a linear relationship between $\Delta\sigma_y$ and $|\delta|$ was observed (see Fig. 13). To monitor the effect of coherency strain on the incremental flow stress, the Mo content was varied in alloys #1,

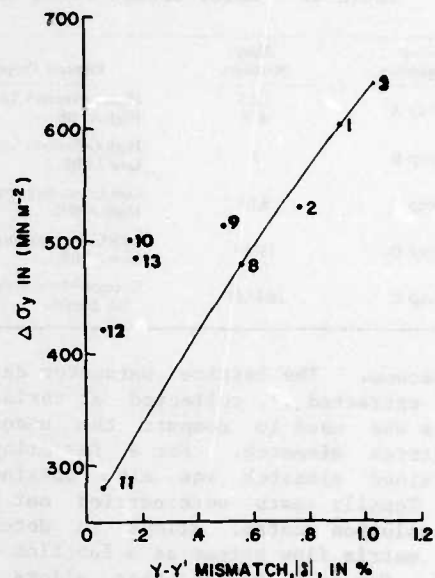


Fig. 13 - Flow stress increment, $\Delta\sigma_y$, vs $\gamma - \gamma'$ mismatch $|\delta|$ (Ref. 32).

2, 9 and 10 from 0 to about 5%. But this also resulted in a concomitant increase in the weight fraction of γ' , and so no linear relationship was found between $\Delta\sigma_y$ and $|\delta|$ for these alloys. If one does not take into account the increase in the incremental flow stress due to weight fraction (from Mo

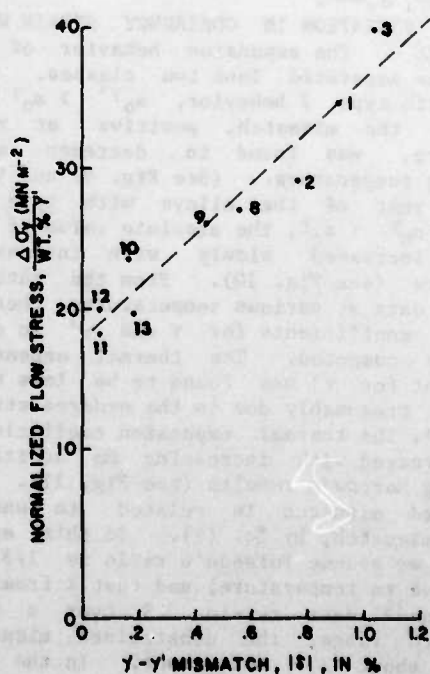


Fig. 14 - Normalized flow stress increment vs $\gamma - \gamma'$ mismatch (Ref. 32).

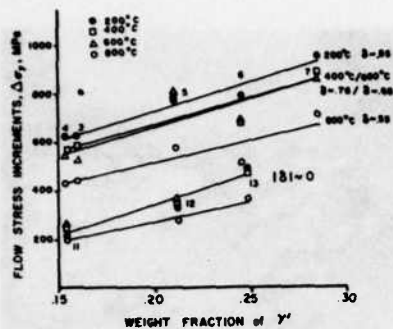


Fig. 15 - Increment in flow stress, $\Delta\sigma_y$, vs weight fraction of γ' for temperature interval 200-800°C.

addition, Ti and Mo, Mo and Al interactions, etc.), the effect of coherency strain will not be evident. But if the flow stress is normalized with respect to weight fraction of γ' , the effect of weight fraction is eliminated and Fig. 14 shows the plot of normalized incremental flow stress vs the $\gamma - \gamma'$ mismatch. The relation between the normalized incremental flow stress and $\gamma - \gamma'$ mismatch is linear.

3.c) TENSILE BEHAVIOR AT HIGH TEMPERATURE - The incremental flow stress $\Delta\sigma_y$ was found to vary linearly with the weight fraction of γ' for a given lattice mismatch (see Fig. 15). This is analogous to the room temperature behavior.

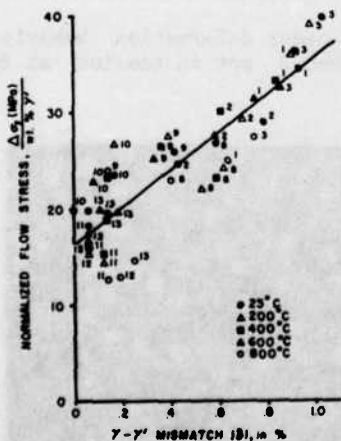


Fig. 16 - Normalized flow stress increment, $\Delta\sigma_y$, vs $\gamma - \gamma'$ mismatch over the temperature range 25°C to 800°C (Ref. 33).

The variation in $\gamma - \gamma'$ mismatch achieved by the Mo addition also affects the weight fraction of γ' . Again, for the high temperature data, the effect of change in weight fraction was eliminated by dividing the incremental flow stress by the weight fraction. This normalized incremental flow stress when plotted versus the $\gamma - \gamma'$ mismatch again shows

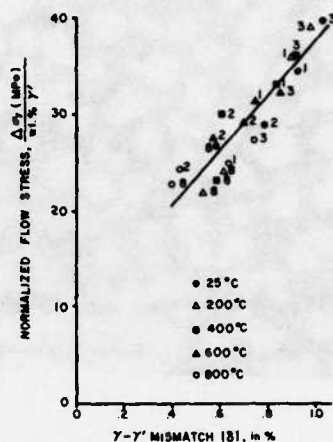


Fig. 17 - Normalized flow stress increment, $\Delta\sigma_y$, vs $\gamma - \gamma'$ mismatch for high coherency alloys (Ref. 33).

the linear relationship, as was observed at room temperature (see Fig. 16).

An interesting point to note here is that in the master plot, Fig. 16 of incremental flow stress vs coherency strain, the greatest degree of scatter is found in group C and D alloys with low coherency strains. A replot of this data for only high coherency alloys (group A and B alloys) is shown in Fig. 17. The excellent linear relationship observed in this figure stresses the coherency strengthening as a dominant strengthening mechanism. Conversely, in group C and D alloys, where the coherency strain is low, the incremental flow strength must be dependent on other strengthening mechanisms (e.g., APBE), and the plot of incremental flow stress versus $\gamma - \gamma'$ mismatch shows wider scatter.

3.d) DISLOCATION-PARTICLE INTERACTION - The dislocation-particle interaction, as seen in TEM samples, determines which mechanism is operating during deformation. The dislocation structure observed after deformation was found to depend upon which group the alloy belonged. The deformation structure can be studied by analyzing a representative alloy in each group.

Deformation structures observed in group D alloys with low coherency strain and low APBE (e.g., #11), deformed at room temperature, at 200°C and at 400°C were similar. The dislocations were paired and a large number of shear bands were observed, indicating particle shear was taking place (see Fig. 18a, 18b and 18c). The dislocation structure in alloy #13 (from same group), after tensile testing at 600°C still showed paired dislocations (Fig. 19). Some dislocations with $a/2 \langle 112 \rangle$ Burger's vector and some super lattice intrinsic/extrinsic faults in γ' were also observed. The dislocation structure in alloy 13 at 800°C, was less planar and a high degree of individual dislocations were observed (see Fig. 20).

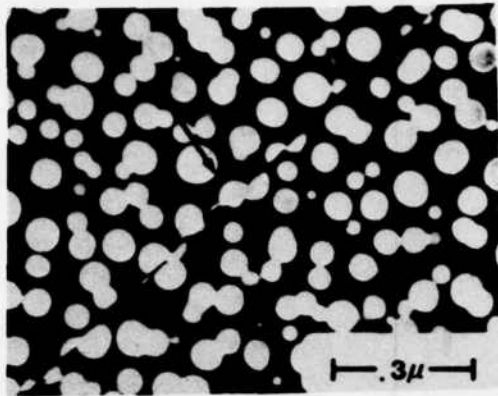


Fig. 19 - Dislocation structure in alloy 13, tension tested at 600°C (Ref. 33).

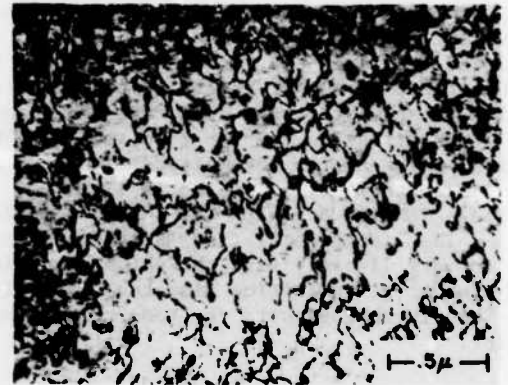
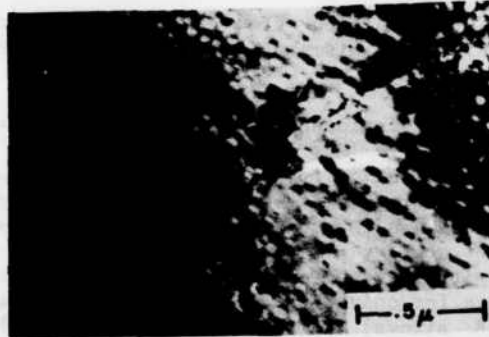
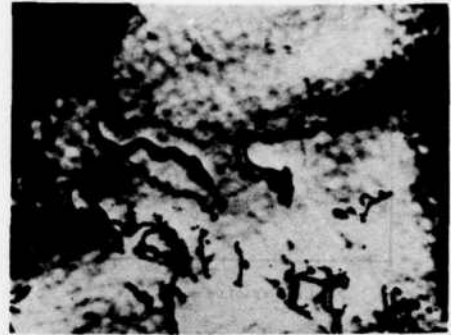


Fig. 20 - Homogeneous deformation behavior of alloy 13, deformed 2 pct in tension at 800°C (Ref. 33).

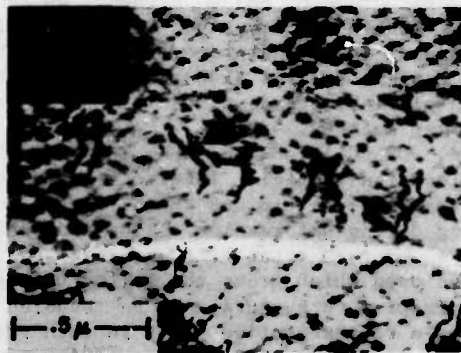


Fig. 18 - γ' particle shear and the dislocation structure in alloy 11 tested at a) room temperature, b) 200°C, and c) 400°C (Ref. 33).

Paired dislocations with significant bowing of the leading dislocation were also seen.

Group C alloys have high APBE and low mismatch. The deformation structure observed after tensile testing at room temperature consisted of shear bands, indicating that particle shear was taking place (Fig. 21). In samples deformed at 200°C, planar arrays of paired dislocations and production of stacking

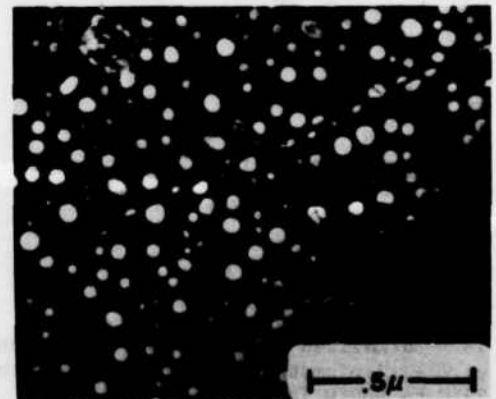


Fig. 21 - Shear band in alloy 10 deformed 2 pct in tension at room temperature. Dark field image using $g = 110$ (Ref. 32).

faults in the γ' were observed. The transition from high energy APB shear to mixed shear (APB and S/ISF and S/ESF) seems to occur at 200°C (see Fig. 22). The dislocation structure at



Fig. 22 - Dislocation structure in alloy 10, tested at 200°C (Ref. 33).



Fig. 23 - Intrinsic/Extrinsic faults observed in γ' particles of alloy 10, tested at 800°C. Dark field image using $g = 010$ (Ref. 33).

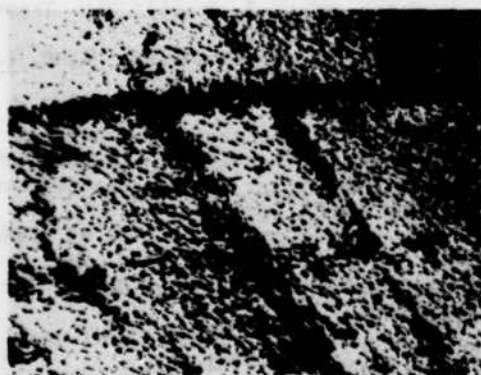


Fig. 24 - Planar slip bands in alloy 1 tested at 200°C (Ref. 33).

400°C and 600°C also contained planar arrays of paired dislocations and sheared γ' particles with faults. The microstructure of alloy #10 tested at 800°C, shows most of the γ' particles containing superlattice intrinsic/



Fig. 25 - Pinched-off residual loops in alloy 1 tested at 800°C. Dark field image using $g = 100$ (Ref. 33).

extrinsic faults (Fig. 23). The thermally activated dissociation of a superlattice dislocation into a pair of partials separated by low energy intrinsic/extrinsic stacking faults must be energetically favorable in this alloy with high ABPE. Most γ' particles were sheared in this manner at 800°C. The existence of matrix stacking faults observed in alloy 10 indicates low stacking fault energy and must be due to the high molybdenum content as discussed earlier.

Group A alloys have high APBE and high coherency strain. The deformation structure of alloy #1 after tensile testing at room temperature showed planar slip bands and residual dislocation loops. No particle shear was observed. At 200°C, similar structure was observed (see Fig. 24). The dislocations were on well defined slip bands and where two slip bands crossed, the dislocations seemed tangled. No particle shear was observed and so no paired dislocations were found. Similar structure was seen in the samples deformed at 400°C, at 600°C and at 800°C. However, only the sample tested at 800°C showed pinched off dislocation loops (see Fig. 25). This could be probably due to decrease in coherency strain at 800°C.

4. DISCUSSION AND SUMMARY

The study of flow stress in a Ni-15Cr-Ti-Al-Mo alloy series clearly demonstrates that coherency strain is a potent strengthening mechanism. The increment in flow stress due to precipitation was found to correlate well to the magnitude of the $\gamma - \gamma'$ mismatch at all temperatures, demonstrating that coherency strain dominates the flow stress. The details of the dislocation-particle interaction does not seem to affect the flow stress. In high coherency alloys, particle bypass by dislocations is observed. In low coherency alloys, particle shear is observed. The particle shear observed in low coherency alloys in the peak-aged condition, could be explained by the order

strengthening model proposed by Reppich,³⁶ in which the peak strength is not attributed to the transition from particle shear to particle bypass, but rather is attributed to a critical particle diameter, where the transition from "weak" pair coupling to "strong" pair coupling occurs. In commercial superalloys, coherency strengthening is generally sacrificed in order to achieve microstructural stability at high temperatures. For low or intermediate temperature service, where the question of particle stability does not arise, coherency strain strengthening can be utilized to achieve maximum strength. In nickel-base superalloys, alloying with group IVB and VB metals (except for vanadium) leads to an increase in the coherency strain, whereas group VIB metals decrease it. Molybdenum is particularly useful in reducing misfit strain. However caution has to be exercised in alloy design, since alloying with Mo also affects the thermal expansion coefficient of γ and γ' , the APBE in γ' , the stacking fault energy in γ and the volume fraction of γ' precipitate.

ACKNOWLEDGEMENT

The authors appreciate the support of the Office of Naval Research, both in the course of this effort and for our research which is reported in this review.

REFERENCES

1. V. Gerold and H. Haberkorn, *Phys. Stat. Sol.*, **16**, p. 675 (1966).
2. H. V. Gleiter, *Z. Agnew Physik*, **23**, p. 108 (1967).
3. R. A. Ricks, A. J. Porter and R. C. Eob, *Acta Met.*, **31**, p. 43 (1983).
4. H. Gleiter, *Mat. Sci. Eng.*, **2**, p. 285 (1967-68).
5. G. C. Weatherly and R. B. Nicholson, *Phil. Mag.*, **17**, p. 801 (1968).
6. L. M. Brown and R. K. Ham, *Strengthening Methods in Crystals*, ed. by A. Kelly and R. B. Nicholson, Appl. Sci. Ltd., London (1971).
7. I. L. Mirkin and O. D. Kanchev, *Met. Sci. and Heat Trans.*, **1-2**, p. 10 (1967).
8. G. N. Maniar, J. E. Bridga, Jr., H. M. James, and G. B. Haydt, *Met. Trans.*, **1**, p. 31 (1970).
9. G. N. Maniar and J. E. Bridga, Jr., *Met. Trans.*, **2**, p. 95 (1971).
10. G. N. Maniar, J. E. Bridga, Jr., and H. M. James, *Met. Trans.*, **2**, p. 1484 (1971).
11. R. G. Davies and T. L. Johnston, "The Metallurgical Design of a Superalloy," Third Bolton Landing Conference, Claitor's Pub. Div. (1970), p. 447.
12. R. Nordheim and N. J. Grant, *J. of Metals*, **6**, p. 211 (1954).
13. J. R. Mihalisin and R. F. Decker, *Trans. AIME*, **218**, p. 507 (1960).
14. R. F. Decker and J. R. Mihalisin, *Trans. ASM*, **62**, p. 481 (1969).
15. P. Nash and D. R. F. West, *Met. Sci.*, **13**, p. 670 (1979).
16. P. Nash and D. R. F. West, *Met. Sci.*, **15**, p. 347 (1981).
17. R. D. Rawlings and A. E. Staton-Bevan, *J. of Mat. Sci.*, **10**, p. 505 (1975).
18. N. S. Stoloff, "Fundamentals of Strengthening," *The Superalloys*, ed. by C. T. Sims and W. C. Hagel, Wiley (1972), p. 95.
19. C. Lall, S. Chin and D. P. Pope, *Met. Trans.*, **10A**, p. 1323 (1979).
20. C. T. Sims, "Cobalt Base Alloys," *The Superalloys*, ed. by C. T. Sims and W. C. Hagel, Wiley (1972), p. 171.
21. J. D. Varia, "Microstructures and Properties of Superalloys," *The Superalloys*, ed. by C. T. Sims and W. C. Hagel, Wiley (1972), p. 231-257.
22. O. H. Kreige and J. M. Baris, *Trans. ASM*, **62**, p. 195 (1969).
23. R. M. N. Pelloux and N. J. Grant, *Trans. AIME*, **218**, p. 232 (1960).
24. T. C. Tierney and N. J. Grant, *Met. Trans.*, **13A**, p. 1827 (1982).
25. A. Akhtar and E. Teghtsoonian, *Met. Trans.*, **2**, p. 2757 (1971).
26. A. Havalda, *Trans. ASM*, **62**, p. 477 (1969).
27. A. Havalda, *Trans. ASM*, **62**, p. 581 (1969).
28. W. T. Loomis, J. W. Freeman and D. L. Sponseller, *Met. Trans.*, **3**, p. 989 (1972).
29. V. Biss and D. L. Sponseller, *Met. Trans.*, **4**, p. 1953 (1973).
30. R. L. Dreshfield and J. F. Wallace, *Met. Trans.*, **5**, p. 71 (1974).
31. H. Morrow III, D. L. Sponseller and M. Semchysheh, *Met. Trans.*, **6A**, p. 477 (1975).
32. R. F. Miller and G. S. Ansell, *Met. Trans.*, **8A**, p. 1979 (1977).
33. D. A. Gross and G. S. Ansell, *Met. Trans.*, **12A**, p. 1631 (1981).
34. K. Ono and R. Starn, *Trans. AIME*, **245**, p. 171 (1969).
35. L. R. Cornwell, J. D. Embury and G. R. Purdy, "The Mechanical Properties of Ni-Al Alloys with Varying Composition," Third Bolton Landing Conference, Claitor's Pub. Div. (1970), p. 387.
36. B. Reppich, *Acta Met.*, **30**, p. 87 (1982).
37. R. S. Mints, G. F. Belyaeva and Y. S. Malkov, *Russ. J. of Inorg. Chem.*, **7**, p. 1236 (1962).
38. A. Taylor and R. W. Floyd, *J. of Inst. of Metals*, **81**, p. 25 (1952-53).
39. R. W. Guard and J. H. Westbrook, *Trans. AIME*, **215**, p. 807 (1959).
40. J. E. Doherty, B. H. Kear and A. F. Glamei, *J. Metals*, **23**, p. 59 (1971).
41. W. B. Pearson, *A Handbook of Lattice Spacings and Structures of Metals and Alloys*, Pergamon Press (1958), pp. 778-779.

This paper is subject to revision. Statements and opinions advanced in papers or discussion are the author's and are his responsibility, not ASM's; however, the paper has been edited by ASM for uniform styling and format.

Printed and Bound by Publishers Choice Book Mfg. Co.
Mars, Pennsylvania 16046

**DAT
FILM**